Composite Structures 238 (2020) 111967

Contents lists available at ScienceDirect

Composite Structures

journal homepage: www.elsevier.com/locate/compstruct

Advanced modeling of lead-free piezocomposites: The role of nonlocal and nonlinear effects

Jagdish A. Krishnaswamy[a,*], Federico C. Buroni[b], Roderick Melnik[a,c], Luis Rodriguez-Tembleque[c], Andres Saez[c]

[a] MS2Discovery Interdisciplinary Research Institute, Wilfrid Laurier University, 75 University Ave W, Waterloo, Ontario N2L 3C5, Canada
[b] Department of Mechanical Engineering and Manufacturing, Universidad de Sevilla, Camino de los Descubrimientos s/n, Seville E-41092, Spain
[c] Department of Continuum Mechanics and Structural Analysis, Universidad de Sevilla, Camino de los Descubrimientos s/n, Seville E-41092, Spain

A B S T R A C T

Lead-free piezocomposites are an ecofriendly route for sensing and harvesting energy from mechanical stimuli and it is important to develop accurate models which can capture essential physical processes underlying their performance. Current piezocomposite design heavily relies on the linear piezoelectric model which neglects nonlocal and nonlinear electro-elastic processes. Here we develop a more accurate modelling paradigm to determine the contributions from nonlocal flexoelectric and nonlinear electrostrictive effects towards the performance of lead-free piezocomposites. We find that in the case of microscale randomly shaped piezoelectric inclusions which represent a practical scenario, the flexoelectric effect does not contribute appreciably towards the piezoelectric response. However, the nonlinear electrostrictive effects impart significant strain-dependent responses. Further, in nano-modified composites, we find that the nonlinear electro-mechanical coupling can have different effects on the transverse and the longitudinal electro-elastic responses. In particular, the longitudinal electric field response, with the nonlinear contribution, is less sensitive to the polycrystalline structure of the piezoelectric inclusions. These observations clearly indicate that at larger strains, nonlinear effects cannot be neglected. In general, our results entail that it is important to include nonlocal and nonlinear processes for reliable and accurate modelling of piezocomposites.

1. Introduction

Lead-free piezocomposites have drawn worldwide attention due to the promise of an environmentally-friendly alternative to lead-based materials for conversion of mechanical stimuli into electrical energy [1,2]. With a clear goal of sustainable technology, at this point lead-free materials lag behind lead-based materials in terms of their performance [2]. The performance issues are typically addressed by tuning the mechanical [3,4], electrical [3–5], and crystalline structural properties [4–7] of the matrix and the piezoelectric inclusions. This includes tuning the hardness of the matrix for better coupling of applied strain to the piezoelectric inclusions [3,4], using nanomaterials such as metal nanoparticles, nanowires, and carbon nanotubes to tune the electrical properties of the matrix to enable better conduction of generated charges to external circuits [3–5], tuning the polycrystallinity of the piezoelectric inclusions to maximize flux generation [4–7] and so on. There have been several efforts to both model and experimentally demonstrate these design pathways. However, in the aspect of design, most of these efforts overlook the contributions due to several important physical effects. These include nonlocal effects such as flexoelectricity and nonlinear effects such as electrostriction. Flexoelectricity refers to the generation of electric flux from strain-gradients, as opposed to flux generation from homogeneous strain which is described by linear piezoelectricity [8–10]. Although flexoelectricity has been explored in the context of a homogeneous material or simple structures [8,11,12], the role of flexoelectricity in practical composite architectures remains to be better understood. Large strain gradients could be expected in composite materials which have hard piezoelectric inclusions in relatively soft matrices and thus the flexoelectric effect could be significant.

The second important electro-elastic process that needs to be considered is electrostriction. This is a nonlinear property of a material by which strains are produced through a quadratic dependence on the electric field [13,14]. A simplistic linear piezoelectric model would predict that the effective strain-normalized response of a piezocomposite (for example its effective e_{ij} coefficients) would be constant, independent of the applied strain. However, nonlinear material behavior could lead to strain-dependent effective material properties. Although the constitutive material laws will not involve any nonlinear (strain-dependent) coefficients, when one considers the dependence of generated electric flux in relation to the applied strains, non-local and electrostrictive processes can give rise to a strain-dependent apparent material behavior. Quantifying both the contributions of the nonlocal and the nonlinear effects, therefore, is an important agenda of this

* Corresponding author.
E-mail address: ajagdish@wlu.ca (J.A. Krishnaswamy).

https://doi.org/10.1016/j.compstruct.2020.111967
Received 25 November 2019; Accepted 17 January 2020
Available online 27 January 2020
0263-8223/

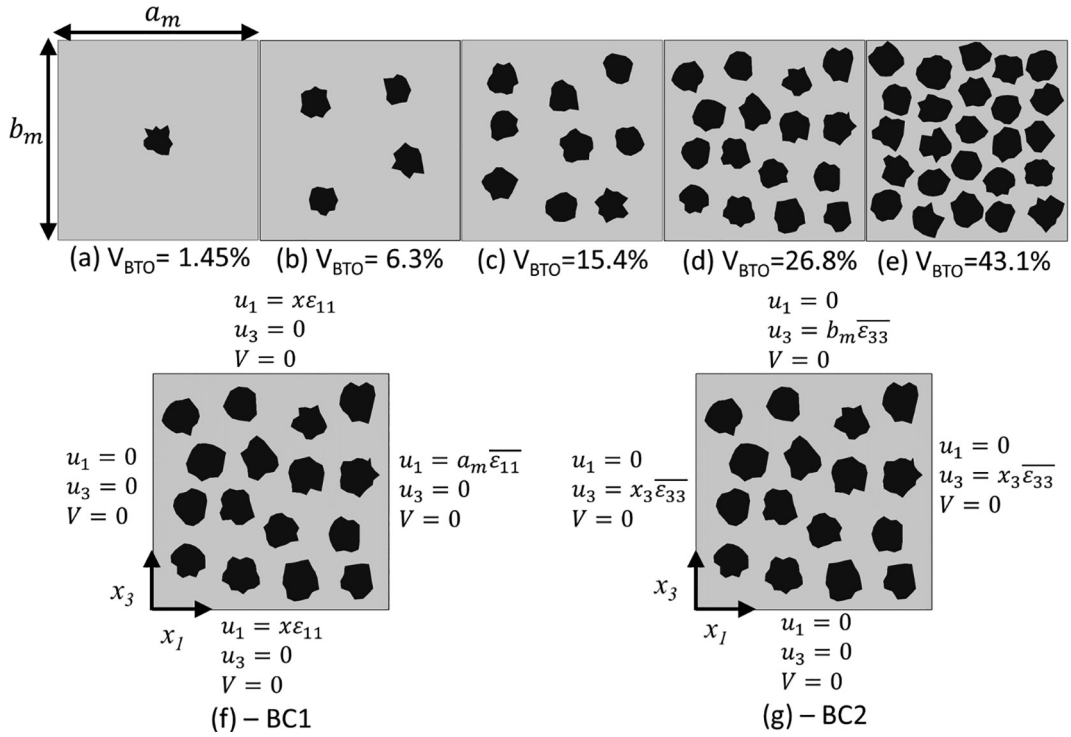

Fig. 1. (a)–(e) Two dimensional RVEs studied in the current investigation with different volume fractions V_{BTO} of $BaTiO_3$ (dark random polygons) embedded in a matrix with sides a_m and b_m, (f) and (g) show the 2 boundary conditions BC1 and BC2, respectively, which are adopted for the current analysis.

paper. We develop a fully coupled electro-elastic model, starting from free-energy considerations, which simultaneously accounts for the linear-piezoelectric, nonlinear and nonlocal effects in a lead-free composite architecture. We first evaluate the contributions of each of these effects towards the electro-elastic response of a two-component piezocomposite consisting of a polymer matrix with embedded piezoelectric micro-sized inclusions. Further, we also evaluate the contribution of these effects in a three-component composite architecture consisting of a CNT-modified matrix with polycrystalline piezoelectric inclusions. The overall objective here is to provide a systematic analysis of the roles and contexts under which the non-local and the nonlinear effects can significantly influence the electro-elastic response.

2. Electro-elastic model, effective electro-elastic coefficients, and boundary conditions

In this section, we will provide the details of the mathematical models that describe the behavior of a piezoelectric composite (Section 2.1) and the boundary conditions used for the determination of the effective electro-elastic coefficients of the composite (Section 2.2). Section 2.2 also further defines the electro-elastic coefficients of principal importance which are investigated in the subsequent sections.

2.1. Electro-elastic model accounting for nonlocal and nonlinear effects

The model developed here will include the effects of strain-gradient electricity or flexoelectricity [10] and electrostriction which is a nonlinear dependence of strain on electric fields [14]. The couplings between the strains, strain-gradients, and electric fields, to capture all these effects, are introduced in a free-energy density function. The Gibbs free energy function which includes all these couplings is given as follows [13,15–17]:

$$G = \frac{1}{2}c_{ijkl}\varepsilon_{ij}\varepsilon_{kl} - \frac{1}{2}\epsilon_{ij}E_iE_j - e_{kij}E_k\varepsilon_{ij} - \frac{1}{2}B_{klij}E_kE_l\varepsilon_{ij} - \mu_{ijkl}E_i\varepsilon_{jk,l} \quad (1)$$

Here, c_{ijkl}, ϵ_{ij}, e_{ijk}, B_{ijkl}, and μ_{ijkl} are the elastic, permittivity, piezoelectric, electrostrictive, and flexoelectric coefficients. Additionally, the field variables include the strain tensor components ε_{ij}, the electric field components E_i and the strain-gradient components $\varepsilon_{jk,l}$. The typical linear piezoelectric models discussed widely in the literature would have only the first three terms on the right-hand side, thus overlooking the nonlocal and nonlinear effects [18].

The phenomenological relations describing the behavior of the composites are derived as follows from Eq (1):

$$\sigma_{ij} = \frac{\partial G}{\partial \varepsilon_{ij}} = c_{ijkl}\varepsilon_{kl} - e_{kij}E_k - \frac{1}{2}B_{klij}E_kE_l \quad (2)$$

$$\hat{\sigma}_{ijk} = \frac{\partial G}{\partial \varepsilon_{ij,k}} = \mu_{lijk}E_l \quad (3)$$

$$D_i = -\frac{\partial G}{\partial E_i} = \epsilon_{ij}E_j + e_{ijk}\varepsilon_{jk} + B_{ijkl}E_j\varepsilon_{kl} + \mu_{ijkl}\varepsilon_{jk,l} \quad (4)$$

Here, σ_{ij}, $\hat{\sigma}_{ijk}$ and D_i are the stress tensor components, the higher order stress tensor components, and electric flux density components, respectively. These constitutive relations are further subjected to the governing balance laws given by [8,11]:

$$(\sigma_{ij} - \hat{\sigma}_{ijk,k})_{,j} + F_i = 0 \quad (5)$$

$$D_{i,i} = 0 \quad (6)$$

where F_i represent the components of the body forces, which are assumed to vanish in our model. The governing equations (Eqs. (5) and (6)) subject to the phenomenological relationships (Eqs. (1) and (2)) are solved using Finite Element Analysis. Also, the strains are related to the displacement components u_i as $\varepsilon_{ij} = \frac{1}{2}(u_{i,j} + u_{j,i})$ and the electric field is related to the electric potential as $E_i = -V_{,i}$. The simulations are carried out on 5 different Representative Volume Elements (RVEs) corresponding to different inclusion volume fractions of $BaTiO_3$, V_{BTO}, as shown in Fig. 1(a)–(e). We select $a_m = b_m = 50\mu$m. The inclusions are randomly shaped and are constrained within concentric circles of radii R_1 and R_2 which are randomly selected within the ranges [2.5–3.5 μm] and [4–5 μm], respectively.

Table 1
Electro-elastic material properties used in the simulations. Typical values of electrostrictive coefficients are considered for the polymer matrix (The flexoelectric coefficients given here are in the experimentally measured range, which are orders of magnitude different from theoretical estimates. Simulations have considered both values).

Material property	Values for $BaTiO_3$	Values for PDMS matrix
Elastic coefficients (Moduli in Pa)		
c_{11}	275.1×10^9 [23]	$\lambda_m + 2\mu_m$
c_{13}	151.55×10^9	λ_m
c_{33}	164.8×10^9	$\lambda_m + 2\mu_m$
c_{44}	54.3×10^9	μ_m
Young's modulus, E_m	N.A.	2×10^6 [24]
Poisson's ratio, ν_m	N.A.	0.499
Relative permittivity		
ϵ_{11}/ϵ_0	1970 [23]	2.72 [24]
ϵ_{33}/ϵ_0	109	2.72
Piezoelectric coefficients (cm^{-2})		
e_{15}	21.3 [23]	Matrix is non-piezoelectric
e_{31}	− 2.69	
e_{33}	3.65	
Flexoelectric coefficients (cm^{-1})		
Longitudinal, μ_{11}	1×10^{-6} [15,16,25]	1×10^{-9} [26]
Transverse, μ_{12}	1×10^{-6} [15,16,27]	1×10^{-9}
Shear, μ_{44}	0	0
Electrostrictive coefficients, Q_{ijkl} (m^4C^{-2}) *or* $M_{ijkl}(V^{-2}m^2)$		
Longitudinal	0.1 $m^4\ C^{-2}$ [28]	$-1 \times 10^{-17}\ V^{-2}\ m^2$ [20]
Transverse	$-0.034\ m^4\ C^{-2}$	0
Shear	0.29 $m^4\ C^{-2}$	0

The material properties adopted for the simulations are summarized in Table 1. For our investigation, we choose a PDMS matrix and polycrystalline $BaTiO_3$ piezoelectric inclusions. We choose microscale piezoelectric inclusions because this would allow grain sizes which lead to optimal polycrystallinity and maximal piezoelectric response [6]. Note that in the case of the flexoelectric coefficients, only the transverse and longitudinal values are considered and these are written as μ_{11} and μ_{13}. These values are characterized on cubic $BaTiO_3$ crystals, the symmetry of which gives only three components – the longitudinal μ_{11}, the transverse μ_{13} and the shear μ_{44} components [19]. Since the shear flexoelectric behavior of $BaTiO_3$ is not well characterized [15], we include only the transverse and the longitudinal components in the model. In our case, we have the longitudinal component and transverse components μ_{11} and μ_{13} defined such that the flexoelectric polarization components generated by strain gradients are given by $P_1 = \mu_{11}\varepsilon_{11,1} + \mu_{13}\varepsilon_{33,1}$ and $P_3 = \mu_{13}\varepsilon_{11,3} + \mu_{11}\varepsilon_{33,3}$ [19].

Secondly, it is important to note that the coefficients of electrostriction mentioned in the model Eqs. (1) and (2), i.e. B_{ijkl} are different from experimentally measured coefficients mentioned in Table 1. Experimentally measured values of electrostrictive coefficients can be expressed in two forms – Q_{ijkl}, the electrostriction measured in terms of the polarization density components P_i, and the M_{ijkl}, the electrostriction measured in terms of the electric field components E_i [20,21]. These are defined as follows [21]:

$$\varepsilon_{ij} = Q_{ijkl}P_kP_l \tag{7a}$$

$$\varepsilon_{ij} = M_{ijkl}E_kE_l. \tag{7b}$$

This means that the strain resulting from electrostriction can be characterized either as a function of the polarization density components P_i or the electric field components E_i. These two forms of representations are interconvertible as $M_{ijkl} = Q_{opkl}\eta_{oi}\eta_{pj}$ [21], where the tensor components η_{ij} correspond to the dielectric susceptibility of the material. Further, the coefficients M_{ijkl} need to be converted to the form required by the model (i.e. B_{ijkl}) as $B_{ijkl} = c_{ijpq}M_{pqkl}$ [22]. Also, the electrostrictive coefficients are measured on materials with cubic symmetry or isotropy, which means that the only coefficients which are non-zero are the longitudinal, transverse, and a shear component, similar to the flexoelectric coefficients. The terms λ_m and μ_m in Table 1 refer to the Lame's constants of the elastically isotropic matrix which are given by $\lambda_m = \frac{E_m\nu_m}{(1+\nu_m)(1-2\nu_m)}$ and $\mu_m = \frac{E_m}{2(1+\nu_m)}$.

2.2. Electro-elastic coefficients of interest and boundary conditions

The system of coordinates along with the two sets of boundary conditions applied here are shown in Fig. 1(f) and (g). The performance of an electro-elastic composite is measured by its ability to simultaneously generate high electric flux and electric fields in response to strain. In fact, the energy density in a piezoelectric material, under strain, is maximized when both the flux and the electric field are maximized [2,29]. Therefore, we define two effective parameters which will measure these quantities. Using the notation $\langle * \rangle$for the volume average of a quantity $*$, and the Voigt notation for the applied strain on the boundary (refer to Fig. 1(f)–(g)), we define these parameters as follows:

$$p_{ij} = \frac{\langle D_i \rangle}{\overline{\varepsilon_j}} \tag{8a}$$

$$\xi_{ij} = \frac{\langle E_i \rangle}{\overline{\varepsilon_j}} \tag{8b}$$

Here, the quantity p_{ij} corresponds to the volume average of the i^{th} component of the electric flux generated in response to the strain component j in the Voigt notation, normalized by the volume averaged strain. Similarly, the quantity ξ_{ij} corresponds to the volume average of the i^{th} component of the electric field generated in response to the strain component j. We will be investigating the components p_{31}, p_{33}, ξ_{31} and ξ_{33}. For example, p_{31} is the volume averaged flux component D_3 generated in response to the volume averaged strain $\overline{\varepsilon_1}$ (which in the usual tensorial notation is $\overline{\varepsilon_{11}}$). Since these quantities are normalized by the applied strain, these are effective electro-elastic parameters. If only linear piezoelectricity is considered, then p_{ij} are the same as the effective piezoelectric coefficients e_{ij}. A different notation is used here to emphasize that the effective coefficients include the nonlocal and nonlinear contributions in addition to the linear piezoelectric contribution. We also emphasize that conventionally effective coefficients are constants that define the response of a material. However, the presence of nonlinear and nonlocal effects in the model can make these coefficients strain-dependent and identifying the nature of this dependence is of particular interest in this paper. Further, we also look at the parameter $\eta_{ij} = p_{ij}\xi_{ij}$, which could be considered as a figure of merit which measures both the effectiveness of flux and field generation, in accordance with other studies seen in the literature [29]. In fact, this parameter is representative of the energy density in the composite under strain [4,29], and designs typically aim to maximize this quantity. Note that the quantities p_{31}, ξ_{31}, and η_{31} are evaluated using the boundary BC1 and the quantities p_{33}, ξ_{33} and η_{33} are evaluated using the boundary condition BC2. BC1 and BC2 are the standard boundary conditions used for the evaluation of the effective piezoelectric coefficients e_{31} and e_{33}, respectively, in traditional linear piezoelectric analysis [30–32]. In fact, the quantities p_{31} and p_{33} are more general definitions which are equal to the quantities e_{31} and e_{33} in the absence of nonlocal and nonlinear considerations. The general modeling paradigm described in this section will be subject to the two-dimensional $x_1 - x_3$ axis system and the cubic symmetry (for inclusions) or isotropic symmetry (for matrix) of the flexoelectric coefficients, μ and the electrostrictive coefficient tensors, Q and M. As mentioned earlier, the cubic symmetry is invoked for the inclusions because of the availability of clear experimental and computational data for this phase, where piezoelectric effects can be ruled out. These simplifications and the reduced model equations which are used for the analysis are summarized in appendix A1. Further, to the boundary conditions on the

displacement and the electric potential mentioned in Fig. 1(f)–(g), we elaborate on the strain gradients on the boundaries in appendix A2. Briefly, the boundary conditions adopted here will calculate flexoelectric contributions only due spatial inhomogeneities in the composite (due to the presence of two components). Flexoelectricity arising from a deliberate external application of inhomogeneous strain or strain gradients occurring due to geometrical anisotropies in the composite architectures at larger scales are not considered here. The focus of this work is to investigate and quantify the contributions of flexoelectricity and electrostriction to the response of geometrically and compositionally homogeneous piezocomposites with microscale lead-free piezoelectric inclusions.

3. Results and discussion

We discuss the results relating to the nonlocal and nonlinear contributions. We do a step-by-step analysis. We start with the linear piezoelectric model and introduce modifications sequentially starting with the flexoelectricity followed by electrostriction. We finally look at the role of electrostriction in nano-modified composites. We accordingly split the discussion into three sub-sections corresponding to these scenarios.

3.1. Nonlocal flexoelectric contribution to the electro-elastic response

We begin by looking at the contribution of the flexoelectric effect alone. For $BaTiO_3$, experimentally measured values of the flexoelectric coefficients are of the order of 1×10^{-6} C/m [15,16,25,27]. However, theoretical predictions suggest much smaller values around 1×10^{-9} C/m [33]. We simulate the response of the composite for both values of the flexoelectric coefficient. The results are plotted in Fig. 2, for different inclusion concentrations V_{BTO}. It is seen that considering the length scales of inclusion geometry, consisting of microscale inclusions, the flexoelectric effect has negligible contributions both to the generated flux (Fig. 2(a)-(b)) and the electric fields (Fig. 2(c)-(d)). This is not surprising, considering that the flexoelectric effect is more sensitive at the nanoscale [19].

Also, a requirement for flexoelectric contributions to be significant in a composite includes the presence of aligned inclusions having geometric anisotropy [8], which is absent in the practical scenario such as that considered here. Further, we have also considered the case where we assume that these RVEs are spatially replicated to build a macroscale structure which has no geometric anisotropy (by specifying no explicit strain gradients – refer appendix A2). While it is known that such geometric anisotropies can produce strain gradients and significant flexoelectricity, we are interested in investigating the role of flexoelectricity in a more practical setting of a homogeneous composite. The randomness in the positions and shapes of the inclusions could however result in a net anisotropy and hence a next flexoelectric effect. However, at the length scales we have considered for this study, the focus of which is restricted to random microscale inclusions which offer the possibility of optimal polycrystallinity and grain size in the submicron-micron scale [5,6] for best piezoelectric performance, we see that flexoelectricity has a negligible effect.

3.2. Nonlinear electrostrictive contribution to the electro-elastic response

We next turn our attention to the nonlinear contribution to the electro-elastic response. In particular, we expect to see strain-dependent effective material coefficients as discussed in Section 2.2. Fig. 3 shows the effective coefficients p_{ij}, ξ_{ij}, and η_{ij} for a representative example of an RVE with the inclusion concentration $V_{BTO} = 43.1\%$. It is clear that the nonlinear effects indeed lead to strain-dependent effective electro-elastic material parameters. In the absence of nonlinear effects these parameters would have been constants. The parameters p_{ij} and ξ_{ij} increase as the volume averaged strain increases, in both the cases of

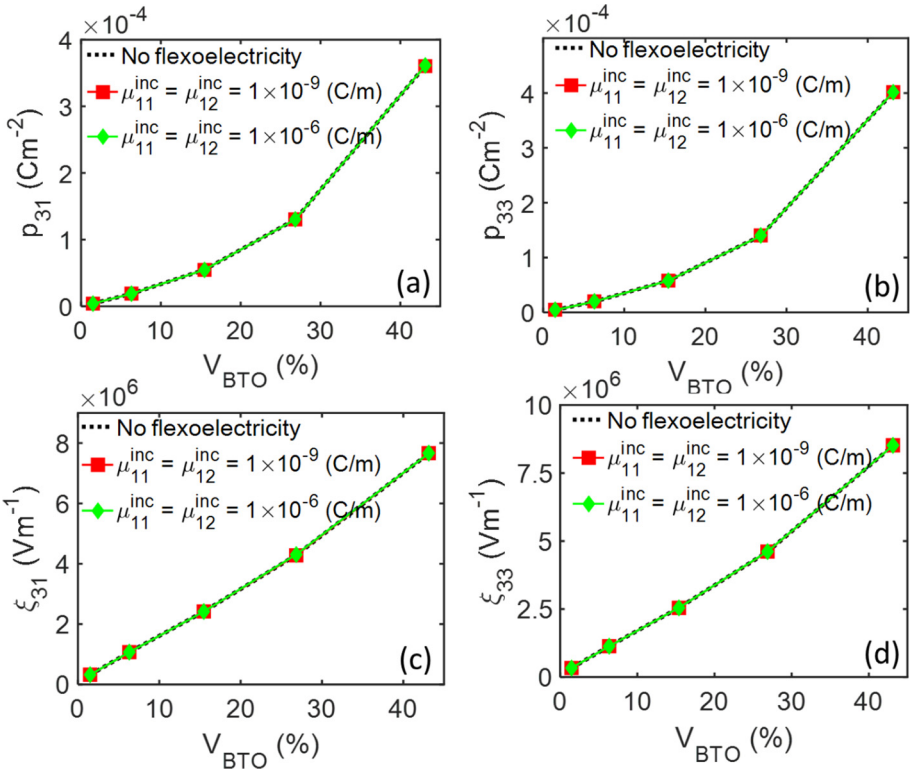

Fig. 2. The effective coefficients for electric flux, p_{31} and p_{33} ((a) and (b), respectively), and for electric field, ξ_{31} and ξ_{33} ((c) and (d), respectively) obtained from the standard linear piezoelectric model (no flexoelectricity) and the advanced model with flexoelectric considerations. Two sets of coefficients are considered, corresponding to theoretical estimates ($\mu_{11}^{inc} = \mu_{12}^{inc} = 1 \times 10^{-9}$) and experimental observations ($\mu_{11}^{inc} = \mu_{12}^{inc} = 1 \times 10^{-6}$), to model the flexoelectricity of $BaTiO_3$. The superscript in μ_{ab}^{inc} refers to the inclusion.

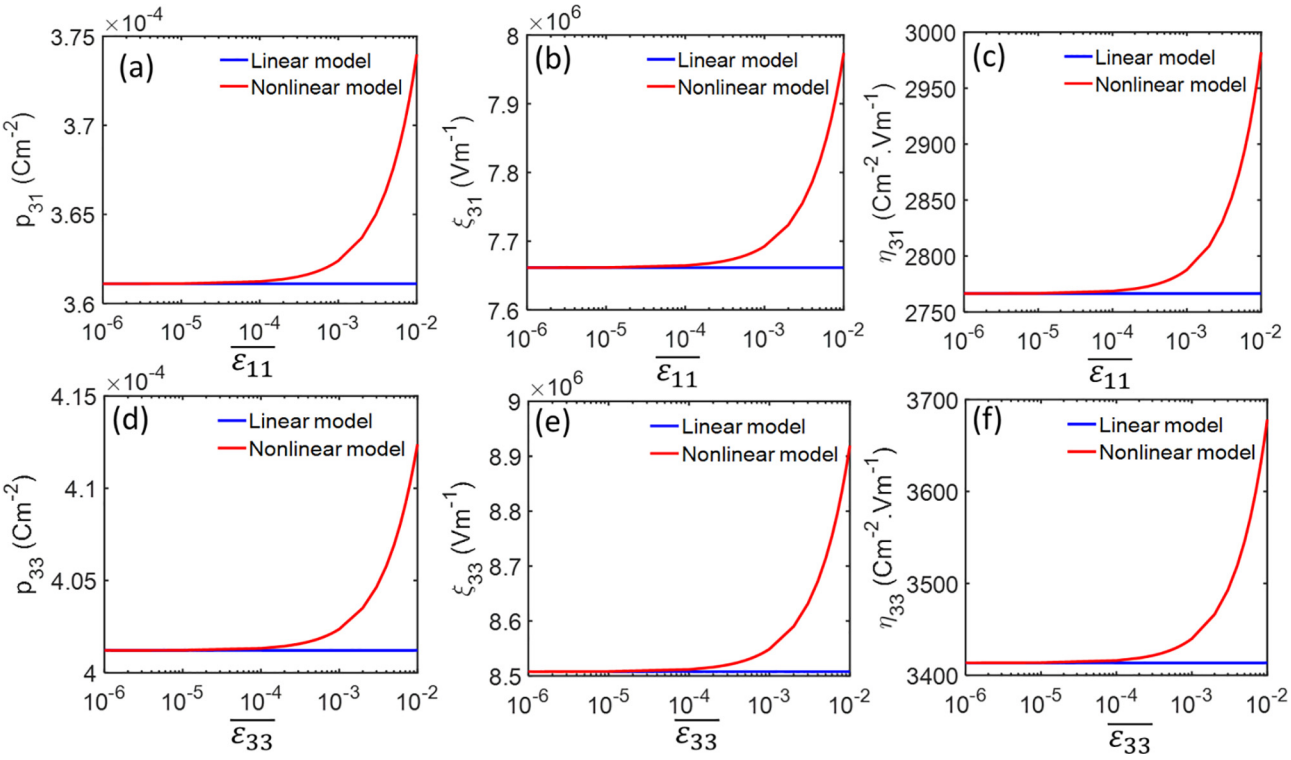

Fig. 3. The effective electroelastic material coefficients, obtained by using boundary conditions BC1 ((a)–(c) corresponding to p_{31}, ξ_{31}, and η_{31} respectively) and BC2 ((d)–(f) corresponding to p_{33}, ξ_{33}, and η_{33} respectively), evaluated with and without nonlinear electrostrictive effects. This is a representative example for $V_{BTO} = 43.1\%$.

applied stimuli. Therefore, the product η_{ij} also increases as the strain increases. This indicates that at larger strains, the composite architecture could exhibit significant nonlinear behaviour with strain-dependent piezoelectric coefficients, which cannot be captured by the linear piezoelectric model alone, as suggested by the plots in Fig. 3. This further means that at larger strains, the nonlinear effects allow for more efficient energy generation, which requires both high electric flux and electric field. This clarifies that at larger strains, design considerations must necessarily include the role of electrostriction.

In fact, we see that at higher strains, significant nonlinear contributions are visible at the interfaces between the inclusions and the matrix, as seen in Fig. 4. The generated electrical potential distributions for the two boundary conditions BC1 (Fig. 4(a)-(b)) and BC2 (Fig. 4(c)-(d)) are shown in Fig. 4, with subfigures (a) and (c) corresponding to the predictions of linear piezoelectricity and subfigures (b) and (d) corresponding to the prediction of the nonlinear electro-elastic model. This is an example simulation, for the purposes of illustration, carried out at relatively larger strains corresponding to $\overline{\varepsilon_{11}} = 0.1$ and $\overline{\varepsilon_{33}} = 0.1$, for boundary conditions BC1 and BC2 respectively. Such strains could also be practical in real-life applications such as in flexible devices. The nonlinear model clearly shows that there is an increased electric potential at the interface between the inclusions and the matrix, suggesting an increased flux generation, due to electrostriction, within the inclusions.

Further, it is important to understand the nature of the strain-dependence exhibited by the effective material parameters. Fig. 5(a)-(b), and (d)-(e) suggests that both the effective parameters p_{ij} and ξ_{ij} show a linear dependence on the applied boundary strain $\overline{\varepsilon_{11}}$ or $\overline{\varepsilon_{33}}$ (which is the volume averaged strain in this case). Further, the first-order coefficient, which determines the slope of the linear dependence, also increases with an increase in the inclusion concentration, as shown in Fig. 5(c) and (e) for the parameters p_{ij} and ξ_{ij}, respectively. This inclusion-induced intensification of nonlinear contributions to the electro-elastic response suggests that the nonlinear contribution is significant through the nonlinear behaviour of the $BaTiO_3$ inclusions rather than that through the matrix. Further, it is interesting to note that parameter η_{ij} also exhibits a linear dependence on the applied strain (Fig. 6(a) and (b) corresponding to η_{31} and η_{33}, respectively). Considering that η_{ij} is the product of two parameters having a linear dependence on strain, it is natural to expect a quadratic dependence on strain for this parameter. However, the second order contribution of strain to η_{ij} is weak and hence we observe a linear variation here also. This means that one could expect a linear improvement in the energy density of a piezoelectric harvester as the operating strain increases. As in the case of p_{ij} and ξ_{ij}, the first-order fit parameter for η_{ij} also increases with an increase in the inclusion concentration V_{BTO} (Fig. 6(c)). It is further observed from Figs. 5(c), (f) and 6(c), that the dependence of the first order fit parameters a_{ij}^{p}, a_{ij}^{ξ}, and a_{ij}^{η} exhibit a cubic dependence on the inclusion concentration V_{BTO}. The details of the corresponding polynomial fits are provided in the appendix A3.

3.3. Nonlinear electrostrictive contribution in nano-modified piezocomposites

As highlighted earlier, an important aspect of piezoelectric composite design is that of using nano-additives to the matrix to modify the mechanical and electrical properties of the matrix for better piezoelectric response. An important and well-known implementation of this design aspect is that of using carbon nanotubes, which exhibit both very high elastic coefficients and excellent electrical conductivity, as fillers to simultaneously harden the matrix and increase its permittivity [3,4]. The hardening leads to better coupling of applied strain to the piezoelectric inclusions and the increased matrix permittivity provides an easy path for the generated electric flux to flow from the inclusion through the matrix, which otherwise is a weak dielectric and thus would impede the passage of flux. It is important to note that the addition of carbon nanotubes to a polymer matrix significantly increases the electrostrictive behaviour of the matrix also [20,34], in addition to

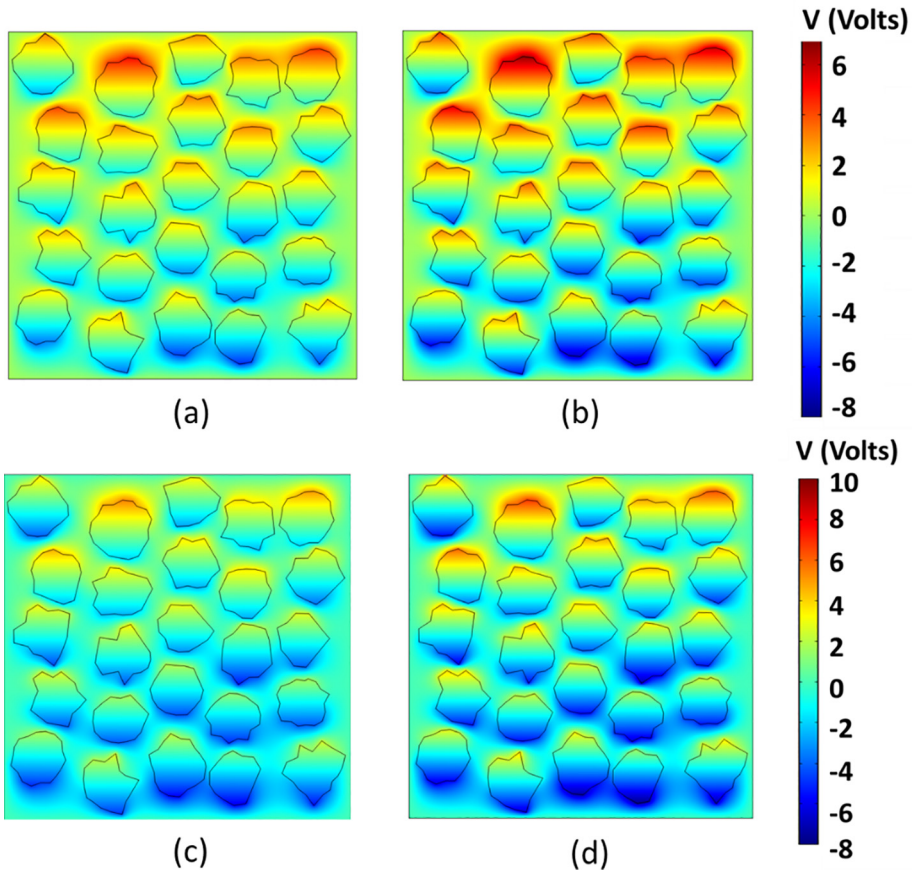

Fig. 4. The electric potential distribution predicted, for an example with $V_{BTO} = 43.1\%$ subject to boundary condition BC1 ((a)-(b)) and BC2 ((c)-(d)). (a) and (b) show the predictions of linear piezoelectricity and (c) and (d) show that of the nonlinear model. In this illustrative example, we have set $\overline{\varepsilon_{11}} = 0.1$ and $\overline{\varepsilon_{33}} = 0.1$ for BC1 and BC2 respectively.

the mechanical and the dielectric properties. The effective electrostriction of such nano-modified matrices can be orders of magnitude higher than the unmodified matrices. This means that it would be important to take into account the nonlinear contribution in nano-modified piezoelectric composites. We consider an example of a PDMS matrix modified by (15,15) MWCNTs. The effective elastic properties of the matrix are obtained using a two-parameter model as detailed in [4,35]. The effective dielectric properties follow a percolation showing a characteristic sudden rise in the permittivity near a critical MWCNT concentration f_{CNT}, called the percolation threshold [36,37]. This dependence of the relative permittivity on f_{CNT} is given by

$$\epsilon_m^{eff} = \epsilon_m \left(\frac{f_c}{f_c - f_{CNT}} \right)^p, \tag{9}$$

where f_c is the percolation threshold, p is the critical exponent, and ϵ_m is the relative permittivity of the pristine matrix.

The percolation threshold for a matrix with uniformly dispersed CNTs, without agglomerations, is around 0.7 (for a nanotube aspect ratio of roughly 100) [36] and the critical exponent p can vary between 0.8 [38] to 1.2 [39], with chemical functionalizing of nanotubes being a proven way to tune these parameters [39]. Typical values of the effective electrostrictive coefficients are taken from the literature. Pristine PDMS exhibits a longitudinal ($M_{1111} = M_{2222} = M_{3333}$) electrostrictive coefficient of -1×10^{-17} m^2 V^{-2} [20]. As carbon nanotubes are added, the value of the coefficient grows while retaining the negative sign up to percolation [20]. For optimally designed matrices with specialized multiscale microstructures having a network of CNT-filled regions running through pristine PDMS, the electrostrictive coefficients can escalate to values as high as -1×10^{-12} m^2 V^{-2} [20]. However, we consider a simpler architecture in which nanotubes are dispersed uniformly in the PDMS matrix, and hence we make a more conservative estimate on the electrostrictive coefficient. We use a value of -1×10^{-15} m^2 V^{-2}, based on experimental observations [40]. Taking all these factors into account, we simulate the behavior of the composite when the matrix is near CNT percolation. The percolation condition is chosen as it is the typical experimental practice to have an electrically well-connected matrix to allow easy passage of electric flux [3]. We apply a boundary strain of $\overline{\varepsilon_{11}} = 5 \times 10^{-3}$or $\overline{\varepsilon_{33}} = 5 \times 10^{-3}$, corresponding to the two boundary conditions discussed in Fig. 1(f)–(g), considering a representative example of $V_{BTO} = 15.4\%$. We further carry out these simulations as a function of the polycrystallinity of the $BaTiO_3$ inclusion. The polycrystallinity of the inclusion is also brought into the design context here because it is seen that when the permittivity of the matrix is enhanced, polycrystalline inclusions could exhibit better piezoelectric response than the single-crystal-based design counterparts [5]. The polycrystallinity is characterized by a parameter α and the effective electroelastic coefficients of polycrystalline $BaTiO_3$ are obtained by weighted orientation averaging as detailed in [23]. We highlight here that very small values of $\alpha (\alpha \to 0)$ correspond to single crystal-like behaviour and very large values ($\alpha \to \infty$) correspond to randomly oriented crystals which exhibit no net piezoelectricity [23]. We see from the Fig. 6 that electrostriction-induced nonlinearity has a different kind of effect on the composite behavior than in the case without nano-modification. First, we notice that the transverse behavior is almost unchanged even in the presence of nonlinear contributions, indicating very small contributions from electrostriction in this case. Both the transverse parameters, p_{31} and ξ_{31} exhibit a similar dependence on the polycrystalline index α as seen from Fig. 7(a)-(b). However, in the longitudinal case (Fig. 7(c)-(d)), the contributions of

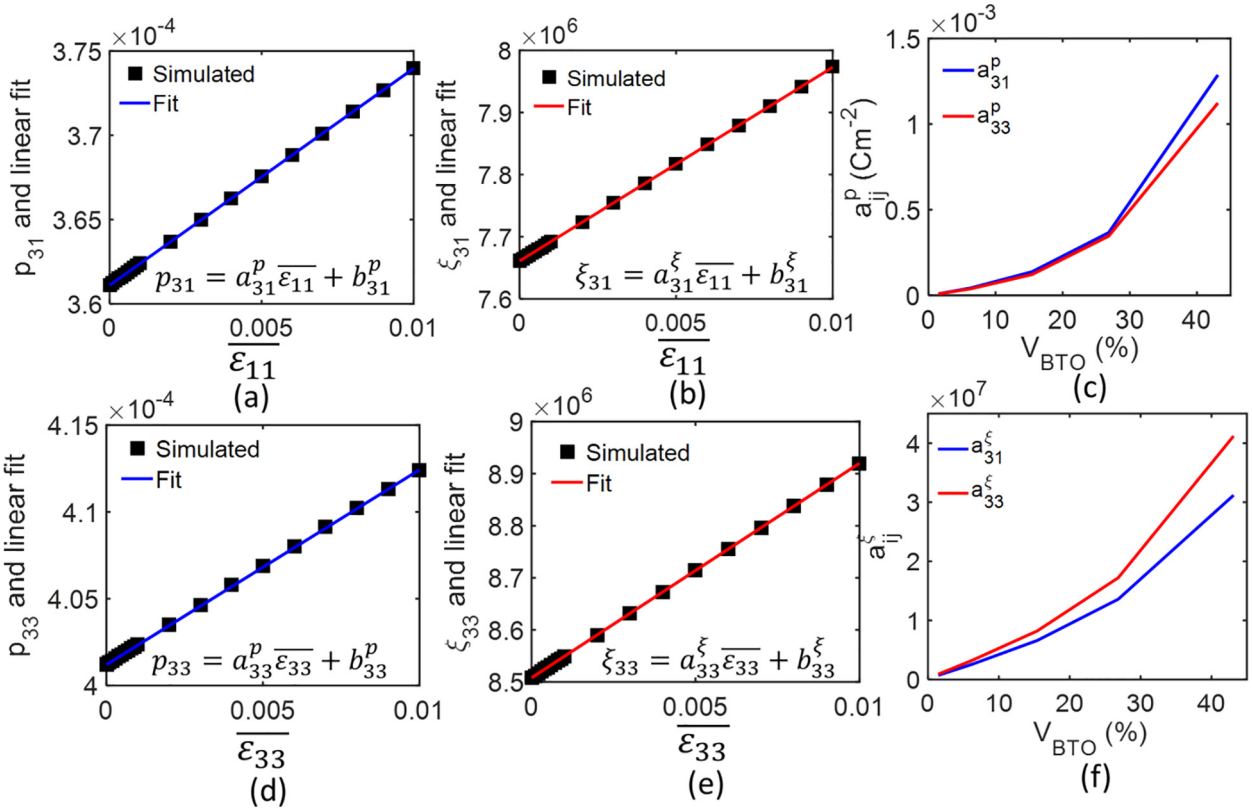

Fig. 5. The linear fits to the calculated parameters (a) p_{31}, (b) ξ_{31}, (d) p_{33}, and (e) ξ_{33}, with the applied boundary strain (or volume averaged strain) $\overline{\varepsilon_{11}}$ or $\overline{\varepsilon_{33}}$ as the independent variable, shown for $V_{BTO} = 43.1\%$. (c) and (f) show the variation of the first order coefficients of the fit as a function of the volume fraction V_{BTO} of the $BaTiO_3$ inclusions.

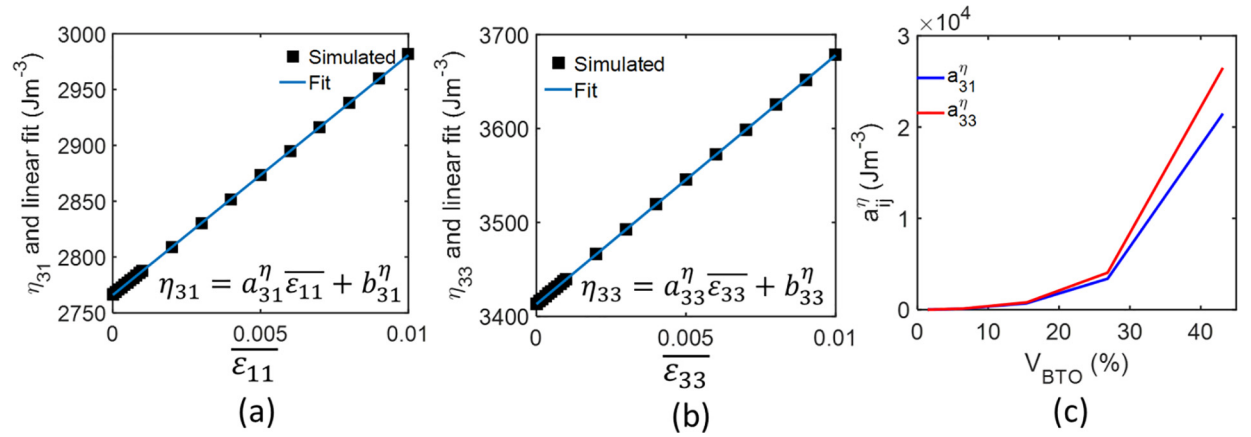

Fig. 6. The linear fit for (a) η_{31} and (b) η_{33} as a function of applied strain, along with the simulated values, as a function of volume averaged strains/applied boundary strains $\overline{\epsilon_{ij}}$, shown for $V_{BTO} = 43.1\%$ (c) The variation of the first order fit coefficient a_{ij}^{η} as a function of the inclusion concentration V_{BTO}.

the electrostrictive processes are significant. It is seen that the nonlinear effects lead to a decrease of electric flux generation (p_{33}), by roughly 18% and an increased electric field generation (ξ_{33}), by around 24%. These differences are quite significant and hence it is important to take into account nonlinear effects while modelling nano-modified piezoelectric composites. Another interesting observation is that with the presence of nonlinear contributions, the electric field generated in the composite (given by ξ_{33}) shows a much weaker dependence on the polycrystallinity of the $BaTiO_3$ inclusions, and remains almost flat over a considerable polycrystalline range (from $\alpha = 0$to $\alpha = 0.2 - 0.3$). This suggests that by choosing an optimum polycrystalline structure, it is possible to maximise the electric flux generation without compromising the electric field characteristics of a single crystal.

In conclusion, in the case of lead-free piezoelectric composites with microscale polycrystalline $BaTiO_3$ inclusions, although flexoelectric effects do not contribute significantly to the response, the nonlinear electrostrictive effects have an appreciable effect. Further, these effects manifest in different ways in nano-modified composites and unmodified composites, thus highlighting the importance of developing advanced mathematical models, accounting for such effects, to accurately predict and design efficient piezoelectric composites. At this point, to the best of our knowledge, there is no experimental literature that evaluates the role of all the three coupled effects discussed here – linear piezoelectricity, flexoelectricity, and electrostriction – in a homogeneous composite material. We, therefore, emphasize that these are first efforts to build advanced models incorporating important electromechanical

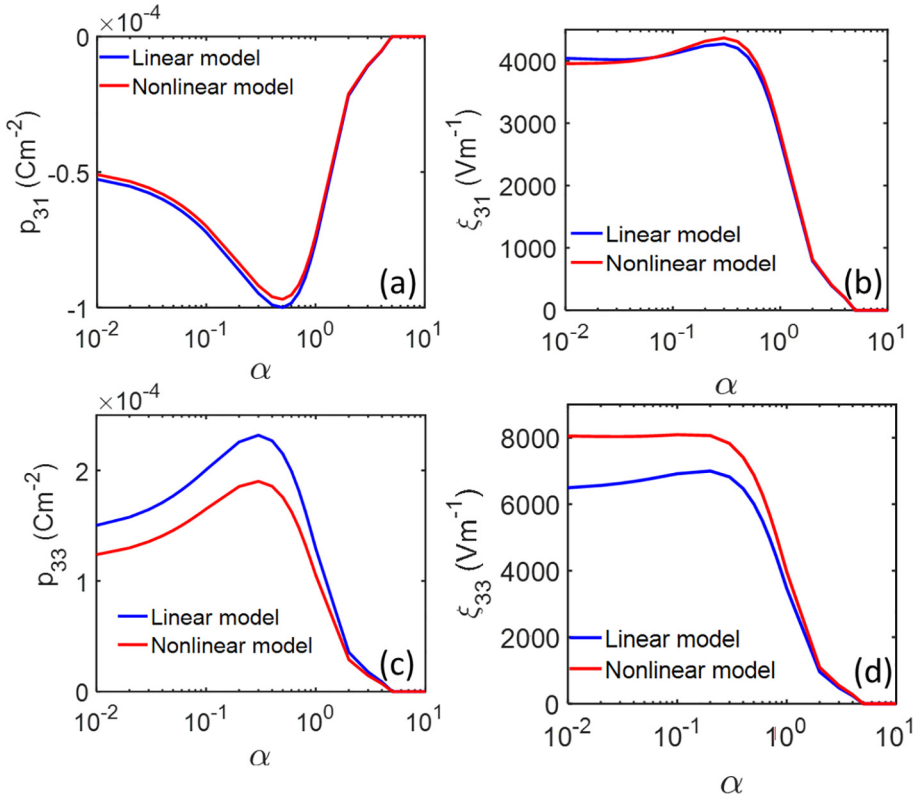

Fig. 7. The effective electric flux and electric field coefficients (a)-(b) p_{31} and ξ_{31}, and (c)-(d) p_{33} and ξ_{33}, as a function of the inclusion polycrystalline index α, calculated with and without nonlinear contributions, for an RVE with $V_{BTO} = 15.4\%$ at an applied strain of $\overline{\varepsilon_{11}} = 0.5 \times 10^{-2}$ (for (a)-(b)) and $\overline{\varepsilon_{33}} = 0.5 \times 10^{-2}$ (for (c)-(d)).

coupled effects, in an attempt to provide direction to design suitable experiments.

4. Summary

We have developed a mathematical paradigm to model piezoelectric composites by taking into account important physical effects such as nonlocal flexoelectric and nonlinear electrostrictive effects. In the composite architectures studied here, comprising of microscale piezoelectric inclusions, flexoelectric effects do not contribute significantly. However, the nonlinear contribution from electrostriction is significant. This leads to emergence of nonlinear effective material parameters characterizing the electric flux and the electric field, which show a linearly increasing dependence on the applied strain. In its turn, this suggests that at larger strains, the contribution to the piezoelectric response due to electrostriction becomes more significant and needs to be taken into consideration in the design. Secondly, the strain-dependence of the effective material parameters characterizing the generated electric flux and fields intensifies with an increase in the inclusion concentration in the composite. This indicates that the nonlinear effects stem predominantly due to the electrostriction within the inclusions rather than in the matrix. Further, in the case of nano-modified composites, comprising of a CNT-modified matrix with polycrystalline piezoelectric inclusions, the electrostrictive effect affects the transverse and the longitudinal electro-elastic response in different ways. While the transverse behaviour is almost unchanged in the presence of the nonlinear effects, the longitudinal behaviour sees a significant reduction in flux generation and a significant improvement in the electric field generation. Additionally, the generated electric field is less sensitive to the polycrystallinity of the inclusion, due to the nonlinear behaviour. These observations provide critical insight into the nonlinear behaviour of piezocomposites and emphasize the importance of developing advanced models to describe electro-elastic behavior. Further, these models can also act as a starting point for the design of efficient piezocomposites and directed experimental efforts to tap into these coupled electromechanical effects to improve piezoelectric performance.

Acknowledgments

This work was supported by the Ministerio de Economía y Competitividad of Spain and the European Regional Development Fund under projects RTI2018-094945-B-C21 and DPI2017-89162-R. The financial support is gratefully acknowledged. RM and AKJ are also grateful to the NSERC and CRC program for their support.

Data availability

The raw data required to reproduce these findings can be made available upon suitable request addressed to the authors.

Appendices

A1: Phenomenological relations in two dimensions

Here we provide the details of the two-dimensional simplification of the model described in Section 2. Because of the cubic symmetry (of the inclusions) or isotropy (of the matrix), a number of flexoelectric and electrostrictive coefficients are zero. This leads to a very simplified model which is detailed below.

The phenomenological equations for the stress components in terms of the strain and the electric fields are

$$\sigma_{11} = c_{11}\varepsilon_{11} + c_{13}\varepsilon_{33} - e_{31}E_3 - \frac{1}{2}B_{1111}E_1^2 - \frac{1}{2}B_{3311}E_3^2 \quad \text{SE(1a)}$$

$$\sigma_{33} = c_{13}\varepsilon_{11} + c_{33}\varepsilon_{33} - e_{33}E_3 - \frac{1}{2}B_{1133}E_1^2 - \frac{1}{2}B_{3333}E_3^2 \quad \text{SE(1b)}$$

$$\sigma_{13} = 2c_{44}\varepsilon_{13} - e_{15}E_1 - \frac{1}{2}B_{1313}E_1E_3 \quad \text{SE(1c)}$$

The higher order stresses arising from flexoelectricity are given by (only non-zero terms listed)

$$\hat{\sigma}_{111} = \mu_{11}E_1 \quad \text{SE(2a)}$$

$$\hat{\sigma}_{113} = \mu_{13}E_3 \quad \text{SE(2b)}$$

$$\hat{\sigma}_{331} = \mu_{13}E_1 \quad \text{SE(2c)}$$

$$\hat{\sigma}_{333} = \mu_{11}E_3 \quad \text{SE(2d)}$$

The electric flux components are given by

$$D_1 = \epsilon_{11}E_1 + \mu_{11}\varepsilon_{11,1} + 2e_{15}\varepsilon_{13} + \mu_{13}\varepsilon_{33,1} + B_{1133}E_1\varepsilon_{33} + B_{1111}E_1\varepsilon_{11} + 2B_{1313}E_3\varepsilon_{13} \quad \text{SE(3a)}$$

$$D_3 = \epsilon_{33}E_3 + e_{31}E_1 + e_{33}E_3 + \mu_{13}\varepsilon_{11,3} + \mu_{11}\varepsilon_{33,3} + B_{3311}E_3\varepsilon_{11} + B_{3333}E_3\varepsilon_{33} + 2B_{3131}E_1\varepsilon_{13} \quad \text{SE(3b)}$$

Here $\mu_{1111} = \mu_{3333} = \mu_{11}$ is the longitudinal flexoelectric coefficient, and $\mu_{1331} = \mu_{3113} = \mu_{13}$ is the shear flexoelectric coefficient. The shear flexoelectric coefficients are assumed to be zero because they are not well characterized experimentally [15]. The electrostrictive coefficients also have similar longitudinal, transverse, and shear coefficients (Q_{ijkl} or M_{ijkl} mentioned in Table 1). These should be further modified as described in Section 2.1 to be used in the above equations as B_{ijkl}. In general, the flexoelectric and electrostrictive data are available for the cubic phase of $BaTiO_3$. Therefore, there are only 3 independent coefficients – the longitudinal, the transverse, and the shear components as shown by the representative matrix below:

$$X = \begin{pmatrix} X_{1111} & X_{1122} & X_{1133} & 0 & 0 & 0 \\ X_{2211} & X_{2222} & X_{2233} & 0 & 0 & 0 \\ X_{3311} & X_{3322} & X_{3333} & 0 & 0 & 0 \\ 0 & 0 & 0 & X_{1313} & 0 & 0 \\ 0 & 0 & 0 & 0 & X_{2323} & 0 \\ 0 & 0 & 0 & 0 & 0 & X_{1212} \end{pmatrix} = \begin{pmatrix} X_{11} & X_{13} & X_{13} & 0 & 0 & 0 \\ X_{13} & X_{11} & X_{13} & 0 & 0 & 0 \\ X_{13} & X_{13} & X_{11} & 0 & 0 & 0 \\ 0 & 0 & 0 & X_{44} & 0 & 0 \\ 0 & 0 & 0 & 0 & X_{44} & 0 \\ 0 & 0 & 0 & 0 & 0 & X_{44} \end{pmatrix} \quad \text{SE(4)}$$

Note that in the above equation, X can either be the flexoelectric coefficient tensor μ, or the electrostrictive coefficient tensor Q or M. Note that the electrostrictive coefficient suitable to the representation in Eqs. SE(1)–(3) is, however, different and the above matrix notation is not suitable to represent it. This is because B is obtained by multiplication with material property tensors which are either anisotropic or non-cubic and thus the above representation breaks down, and B_{ijkl} notation has to be retained. Eqs. SE(1)–(3) are, as already mentioned in Section 2.1, subject to the equilibrium and charge balance laws and appropriate boundary conditions, to obtain the required electro-elastic coefficients. For the matrix, we assume that the transverse and the shear components are equal for both the flexoelectric and the electrostrictive coefficients.

A2: Strain gradients at the boundaries

We will here discuss about the strain gradient values at the boundaries of the RVE. We do not directly specify the strain gradients. The boundary conditions BC1 and BC2 specify the displacement at the boundaries as seen from Fig. 1(f)–(g). As a result of the boundary conditions applied, the strain gradients along the boundaries are determined to be zero in some cases, and in other cases, will be determined by the solution. The Table AT1 specifies which of the strain gradient components are decided by the applied boundary conditions (denoted by their determined value, 0) and which of the components will be determined by the solution (denoted by "–"). The Fig. AF1 shows a reference RVE with the names of the boundaries that will be described by Table AT1.

We particularly note that in the case of BC1, the volume of average of $\varepsilon_{11,1}$ will be zero. Similarly, in the case of BC2, the volume average of $\varepsilon_{33,3}$ will be zero. The physical implication of this is that we calculate the flexoelectricity occurring due to electromechanical variations occurring because of the inhomogeneity in the RVE rather than due to a deliberate external application of a strain gradient. Application of such deliberate strain-

Table AT1
The strain gradients at the boundaries determined partly by the boundary conditions.

Boundary condition	Boundary	$\varepsilon_{11,1}$	$\varepsilon_{11,3}$	$\varepsilon_{13,1}$	$\varepsilon_{13,3}$	$\varepsilon_{33,1}$	$\varepsilon_{33,3}$
BC1	Left	–	0	–	0	0	0
	Right	–	0	–	0	0	0
	Top	0	–	–	–	0	–
	Bottom	0	–	–	–	0	–
BC2	Left	–	0	–	–	–	0
	Right	–	0	–	–	–	0
	Top	0	0	0	–	0	–
	Bottom	0	0	0	–	0	–

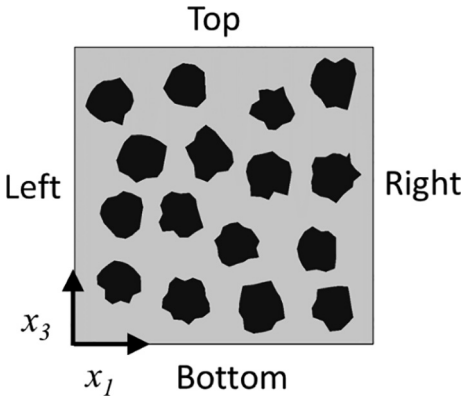

Fig. AF1. The nomenclature used for the 4 boundaries of the RVE described in Table AT1.

gradients will require modifications of the boundary conditions to introduce higher order functions for the boundary displacements.

A3: Polynomial fits of simulated data as a function of inclusion concentration

As explained in Section 3, the electroelastic coefficients p_{ij}, ξ_{ij}, and η_{ij}exhibit a linearly increasing strain-dependence as follows:

$$p_{ij} = a_{ij}^{p}\overline{\varepsilon_{jj}} + b_{ij}^{p},\ \xi_{ij} = a_{ij}^{\xi}\overline{\varepsilon_{jj}} + b_{ij}^{\xi},\ \eta_{ij} = a_{ij}^{\eta}\overline{\varepsilon_{jj}} + b_{ij}^{\eta}. \quad \text{SE(5)}$$

It was also further observed that the first order coefficients, a_{ij}^{p}, a_{ij}^{ξ}, and a_{ij}^{η} increase nonlinearly with respect to the inclusion concentration V_{BTO}. Here we provide the details of the polynomial fits to these data, corresponding to Figs. 4(c), (f), and 5(c). We see that the fit coefficients exhibit a third order dependence on the inclusion concentration (V_{BTO} expressed as a percentage). The fit equations are given below, and the fits are plotted along with the simulated data in Fig. AF2.

$$a_{31}^{p} = 2.025\times10^{-8}V_{BTO}^{3} - 4.34\times10^{-7}V_{BTO}^{2} + 1.111\times10^{-5}V_{BTO} - 9.127\times10^{-6}, \quad \text{SE(6a)}$$

$$a_{33}^{p} = 1.335\times10^{-8}V_{BTO}^{3} - 1.276\times10^{-7}V_{BTO}^{2} + 6.769\times10^{-6}V_{BTO} - 1.78\times10^{-6}, \quad \text{SE(6b)}$$

$$a_{31}^{\xi} = 226.5V_{BTO}^{3} - 2428V_{BTO}^{2} + 4.038\times10^{5}V_{BTO} + 1.293\times10^{5}, \quad \text{SE(6c)}$$

$$a_{33}^{\xi} = 343.7V_{BTO}^{3} - 4611V_{BTO}^{2} + 5.114\times10^{5}V_{BTO} + 1.752\times10^{5}, \quad \text{SE(6d)}$$

$$a_{31}^{\eta} = 0.5431V_{BTO}^{3} - 15.55V_{BTO}^{2} + 165.1V_{BTO} - 285.3, \quad \text{SE(6e)}$$

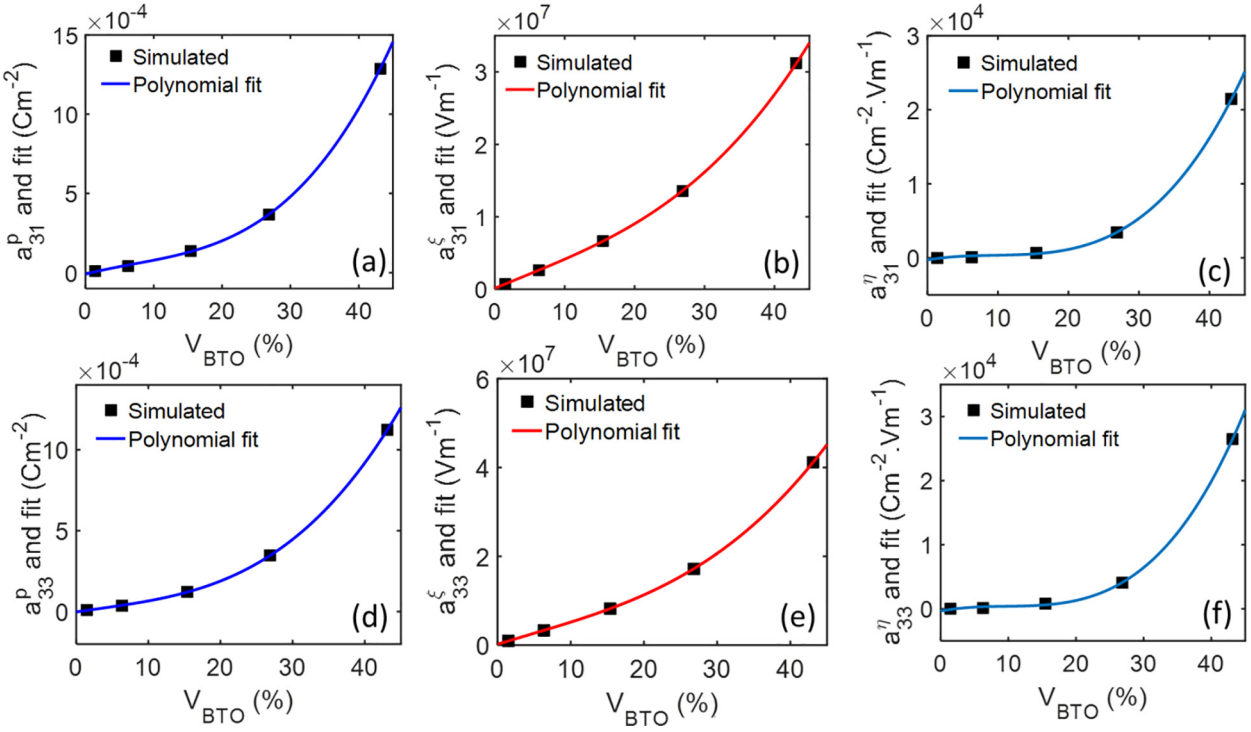

Fig. AF2. The polynomial fits of the simulated variation of the first-order coefficients a_{ij}^{p}, a_{ij}^{ξ},and a_{ij}^{η} as a function of V_{BTO}.

$$a_{33}^{\eta} = 0.6822V_{BTO}^3 - 19.74V_{BTO}^2 + 205V_{BTO} - 352.3. \quad \text{SE(6f)}$$

References

[1] Ibn-Mohammed T, Koh S, Reaney I, Sinclair D, Mustapha K, Acquaye A, et al. Are lead-free piezoelectrics more environmentally friendly? MRS Commun 2017;7:1–7.
[2] Maurya D, Peddigari M, Kang M-G, Geng LD, Sharpes N, Annapureddy V, et al. Lead-free piezoelectric materials and composites for high power density energy harvesting. J Mater Res 2018;33:2235–63.
[3] Kim H, Torres F, Islam MT, Islam MD, Chavez LA, Garcia Rosales CA, et al. Increased piezoelectric response in functional nanocomposites through multiwall carbon nanotube interface and fused-deposition modeling three-dimensional printing. MRS Commun 2017;7:960–6.
[4] Krishnaswamy JA, Buroni FC, Garcia-Sanchez F, Melnik RVN, Rodriguez-Tembleque L, Saez A. Lead-free piezocomposites with CNT-modified matrices: accounting for agglomerations and molecular defects. Compos Struct 2019;224:111033.
[5] Krishnaswamy JA, Buroni FC, Garcia-Sanchez F, Melnik RVN, Rodriguez-Tembleque L, Saez A. Improving the performance of lead-free piezoelectric composites by using polycrystalline inclusions and tuning the dielectric matrix environment. Smart Mater Struct 2019.
[6] Zheng P, Zhang J, Tan Y, Wang C. Grain-size effects on dielectric and piezoelectric properties of poled BaTiO3 ceramics. Acta Mater 2012;60:5022–30.
[7] Maurya D, Zhou Y, Yan Y, Priya S. Synthesis mechanism of grain-oriented lead-free piezoelectric Na0.5Bi0.5TiO3–BaTiO3 ceramics with giant piezoelectric response. J Mater Chem C 2013:2102–11.
[8] Sharma N, Landis CM, Sharma P. Piezoelectric thin-film superlattices without using piezoelectric materials. J Appl Phys 2010;108:024304.
[9] Zubko P, Catalan G, Tagantsev AK. Flexoelectric effect in solids. Annu Rev Mater Res 2013;43.
[10] Yudin P, Tagantsev A. Fundamentals of flexoelectricity in solids. Nanotechnology 2013;24:432001.
[11] Mao S, Purohit PK. Insights into flexoelectric solids from strain-gradient elasticity. J Appl Mech 2014;81:081004.
[12] Liang X, Hu S, Shen S. Effects of surface and flexoelectricity on a piezoelectric nanobeam. Smart Mater Struct 2014;23:035020.
[13] Bahrami-Samani M, Patil SR, Melnik RVN. Higher-order nonlinear electromechanical effects in wurtzite GaN/AlN quantum dots. J Phys: Condens Matter 2010;22:495301.
[14] Sundar V, Newnham R. Electrostriction and polarization. Ferroelectrics 1992;135:431–46.
[15] Abdollahi A, Peco C, Millan D, Arroyo M, Arias I. Computational evaluation of the flexoelectric effect in dielectric solids. J Appl Phys 2014;116:093502.
[16] He B, Javvaji B, Zhuang X. Characterizing flexoelectricity in composite material using the element-free Galerkin method. Energies 2019;12:271.
[17] Kuang Z-b. Internal energy variational principles and governing equations in electroelastic analysis. Int J Solids Struct 2009;46:902–11.
[18] Prabhakar S, Melnik RVN, Neittaanmäki P, Tiihonen T. Coupled magneto-thermo-electromechanical effects and electronic properties of quantum dots. J Comput Theor Nanosci 2013;10:534–47.
[19] Nguyen TD, Mao S, Yeh YW, Purohit PK, McAlpine MC. Nanoscale flexoelectricity. Adv Mater 2013;25:946–74.
[20] Luna A, Pruvost M, Yuan J, Zakri CC, Neri W. Giant electrostrictive response and piezoresistivity of emulsion templated nanocomposites. Langmuir 2017;33:4528–36.
[21] Parulkar WD. Electromechanical characterization of poly (dimethyl siloxane) based electroactive polymers; 2005.
[22] Joshi SP. Non-linear constitutive relations for piezoceramic materials. Smart Mater Struct 1992;1:80.
[23] Li JY. The effective electroelastic moduli of textured piezoelectric polycrystalline aggregates. J Mech Phys Solids 2000;48:529–52.
[24] Johnston I, McCluskey D, Tan C, Tracey M. Mechanical characterization of bulk Sylgard 184 for microfluidics and microengineering. J Micromech Microeng 2014;24:035017.
[25] Hu T, Deng Q, Liang X, Shen S. Measuring the flexoelectric coefficient of bulk barium titanate from a shock wave experiment. J Appl Phys 2017;122:055106.
[26] Chu B, Salem D. Flexoelectricity in several thermoplastic and thermosetting polymers. Appl Phys Lett 2012;101:103905.
[27] Ma W, Cross LE. Flexoelectricity of barium titanate. Appl Phys Lett 2006;88:232902.
[28] Wang J, Meng F, Ma X, Xu M, Chen L. Lattice, elastic, polarization, and electrostrictive properties of BaTiO 3 from first-principles. J Appl Phys 2010;108:034107.
[29] Priya S. Criterion for material selection in design of bulk piezoelectric energy harvesters. IEEE Trans Ultrason Ferroelectr Freq Control 2010;57:2610–2.
[30] Saputra AA, Sladek V, Sladek J, Song C. Micromechanics determination of effective material coefficients of cement-based piezoelectric ceramic composites. J Intell Mater Syst Struct 2018;29:845–62.
[31] Qin R-S, Xiao Y, Lan H. Numerical simulation of effective properties of 3D piezoelectric composites. J Eng 2014;2014.
[32] Sladek J, Sladek V, Krahulec S, Song C. Micromechanics determination of effective properties of voided magnetoelectroelastic materials. Comput Mater Sci 2016;116:103–12.
[33] Xu T, Wang J, Shimada T, Kitamura T. Direct approach for flexoelectricity from first-principles calculations: cases for SrTiO3 and BaTiO3. J Phys: Condens Matter 2013;25:415901.
[34] Deshmukh S, Ounaies Z. Single walled carbon nanotube (SWNT)–polyimide nanocomposites as electrostrictive materials. Sens Actuators, A 2009;155:246–52.
[35] Rodríguez-Tembleque L, García-Macías E, Sáez A. CNT-polymer nanocomposites under frictional contact conditions. Compos B Eng 2018;154:114–27.
[36] Bao H-D, Sun Y, Xiong Z-Y, Guo Z-X, Yu J. Effects of the dispersion state and aspect ratio of carbon nanotubes on their electrical percolation threshold in a polymer. J Appl Polym Sci 2013;128:735–40.
[37] Li J, Ma PC, Chow WS, To CK, Tang BZ, Kim JK. Correlations between percolation threshold, dispersion state, and aspect ratio of carbon nanotubes. Adv Funct Mater 2007;17:3207–15.
[38] Wang F, Wang J-W, Li S-q, Xiao J. Dielectric properties of epoxy composites with modified multiwalled carbon nanotubes. Polym Bull 2009;63:101–10.
[39] Li Q, Xue Q, Hao L, Gao X, Zheng Q. Large dielectric constant of the chemically functionalized carbon nanotube/polymer composites. Compos Sci Technol 2008;68:2290–6.
[40] Park C, Kang JH, Harrison JS, Costen RC, Lowther SE. Actuating single wall carbon nanotube–polymer composites: intrinsic unimorphs. Adv Mater 2008;20:2074–9.